HHS Public Access

Author manuscript

J Physiol. Author manuscript; available in PMC 2023 February 14.

Published in final edited form as:

J Physiol. 2021 February ; 599(3): 943–962. doi:10.1113/JP280656.

Passive stiffness of fibrotic skeletal muscle in *mdx* mice relates to collagen architecture

Sarah E. Brashear[1], **Ross P. Wohlgemuth**[1], **Gabriella Gonzalez**[1], **Lucas R. Smith**[1,2]

[1]Department of Neurobiology, Physiology, and Behavior, University of California Davis

[2]Department of Physical Medicine and Rehabilitation, University of California Davis

Abstract

Fibrosis is prominent in many skeletal muscle pathologies including dystrophies, neurological disorders, cachexia, chronic kidney disease, sarcopenia and metabolic disorders. Fibrosis in muscle is associated with decreased contractile forces and increased passive stiffness that limits joint mobility leading to contractures. However, the assumption that more fibrotic material is directly related to decreased function has not held true. Here we utilize novel measurement of extracellular matrix (ECM) and collagen architecture to relate ECM form to muscle function. We used *mdx* mice, a model for Duchenne muscular dystrophy that becomes fibrotic, and wildtype mice. In this model, extensor digitorum longus (EDL) muscle was significantly stiffer, but with similar total collagen, while the soleus muscle did not change stiffness, but increased collagen. The stiffness of the EDL was associated with increased collagen crosslinking as determined by collagen solubility. Measurement of ECM alignment using polarized light microscopy showed a robust relationship between stiffness and alignment for wildtype muscle that broke down in *mdx* muscles. Direct visualization of large collagen fibres with second harmonic generation imaging revealed their relative abundance in stiff muscles. Collagen fibre alignment was linked to stiffness across all muscles investigated and the most significant factor in a multiple linear regression-based model of muscle stiffness from ECM parameters. This work establishes novel characteristics of skeletal muscle ECM architecture and provides evidence for a mechanical function of collagen fibres in muscle. This finding suggests that anti-fibrotic strategies to enhance muscle function and excessive stiffness should target large collagen fibres and their alignment rather than total collagen.

Keywords

biomechanics; collagen; extracellular matrix; fibrosis; skeletal muscle

Corresponding author Lucas R. Smith: University of California, Davis, 196 Briggs Hall NPB, One Shields Ave, Davis, CA 95616-5270. lucsmith@ucdavis.edu.

Author contributions

Conception and design: S.E.B., L.R.S.; Data collections: S.E.B., R.P.W., L.R.S.; Data analysis and interpretation: S.E.B., R.P.W., G.G., L.R.S.; Drafting of manuscript: S.E.B., R.P.W., L.R.S.; Figure development: S.E.B., R.P.W., G.G., L.R.S.; Critical revision and final approval of manuscript: S.E.B., R.P.W., G.G., L.R.S.

Competing interests

The authors declare that they have no conflicts of interest.

Supporting information

Additional supporting information may be found online in the Supporting Information section at the end of the article.

Introduction

Skeletal muscle's primary function is to produce active contractile force, which is often used to power joint rotation. However, to accommodate joint motion, antagonist muscles must be sufficiently compliant. The end of joint range of motion is often set by the increasing muscle stiffness during stretch; for example, hamstring stiffness determines maximum knee extension when the hips are flexed (Magnusson et al. 2007; Miyamoto et al. 2018). Skeletal muscle passive forces are highly non-linear with respect to stretch and increase rapidly at high strains to prevent damage caused by overstretching muscle (IE et al. 1996; Calvo et al. 2010). Skeletal muscle is also viscoelastic, such that the stiffness is dependent on the velocity of stretch (Myers et al. 1998; Meyer et al. 2011), which is a particularly important consideration in dynamic skeletal muscle. While muscle passive mechanics typically provide a fully functional range of motion, in the context of diseases in which muscle is impacted, the functional range of motion is often reduced, resulting in a muscle contracture (Halar et al. 1978; Nuckolls et al. 2020). Thus, a fixed muscle contracture is the result of excessive passive muscle stiffness. Muscle contracture is a prevalent feature of cerebral palsy (Mathewson & Lieber, 2015; Pingel et al. 2017) and muscle dystrophies (McDonald, 1998; Skalsky & McDonald, 2012) and is a critical cause of disability in these patients (Choi et al. 2018; Lieber & Fridén, 2019). Despite the importance of muscle passive mechanical properties in determining joint functionality, quantitative determinants of muscle passive stiffness are largely unknown.

A common feature of diseases that are complicated by muscle contracture is a pathological increase in extracellular matrix (ECM) components termed fibrosis (Smith & Barton, 2018; Mahdy, 2019). For healthy muscle the relative importance of the ECM to the intracellular structures, namely titin, in determining passive stiffness is still under investigation (HERBERT, 1988; Meyer & Lieber, 2018; Brynnel et al. 2018; Freundt & Linke, 2019; Ward et al. 2020). In fibrotic muscle, however, there is no evidence to show a change in muscle fibre or titin stiffness (Smith et al. 2011; Bates et al. 2013), but there is clearly a disruption of the ECM. Many fibrotic diseases are associated with increased tissue stiffness – an important predictor of disease progression in liver fibrosis (Georges et al. 2007; Carríon et al. 2010). Collagen is the most abundant constituent of the ECM, and fibrillar collagens are known to be the primary load-bearing structures (Fratzl et al. 1998; Gillies & Lieber, 2011). For the most abundant collagen, type I, transcript level indeed scales well with elastic stiffness across tissues in the body (Swift et al. 2013). Surprisingly, however, the amount of collagen is a poor predictor of stiffness in fibrotic muscles from mice (Smith & Barton, 2014). This implicates factors beyond the abundance of ECM in fibrosis that contribute to excessive muscle stiffness.

Collagen undergoes extensive post-translational modifications which facilitate its incorporation into the fibrillar matrix and modify ECM stiffness. Collagen crosslinking is one such modification, which increases the stiffness of collagen fibres and has been associated with tissue stiffness in multiple fibrotic conditions (Norton et al. 1997; Georges et al. 2007; Jones et al. 2018). While evidence of extensive collagen crosslinking has been reported in dystrophic patients and animal models (Smith et al. 2016), accounting for

collagen crosslinking did not improve predictability of passive stiffness in a fibrotic mouse model (Chapman et al. 2015). There are many constituents of the ECM in muscle that may influence ECM stiffness directly or through altering the architecture of the fibrillar collagen network (Bonnans et al. 2014; Lampi & Reinhart-King, 2018). An extensive proteomic analysis was able to account for a large degree of stiffness in muscle contractures from patients with cerebral palsy (Smith et al. 2019); however, the dominating factor was the ratio of type I to type III collagen, implicating a reorganization of the ECM rather than an individual component having a direct effect. Beyond biochemical characterization of the ECM, the orientation of the ECM is known to be an important factor in determining network mechanics (Wang et al. 2015; Taufalele et al. 2019). In tendons it is well appreciated that decreased alignment of collagen yields a decreased stiffness (Lake et al. 2009; Miller et al. 2012; Riggin et al. 2014). However, the alignment of collagen fibres in skeletal muscle is unknown, particularly in the case of fibrotic diseases with excessive stiffness.

We hypothesized that skeletal muscle's elastic and viscous passive mechanical properties would scale not with collagen content, but with collagen crosslinking and collagen alignment. Here we tested the hypothesis using a mouse model of muscular dystrophy, the *mdx* mouse, on a genetic background that generates a more profound fibrotic phenotype (van Putten et al. 2019). Multiple muscles were examined using established passive mechanical testing in conjunction with biochemical assays for collagen content and crosslinking (Smith & Barton, 2014; Smith et al. 2016). Advanced imaging modalities in conjunction with specific analysis for muscle tissue were conducted to robustly evaluate collagen alignment in the same muscle samples. Rotational linearly polarized light microscopy was used as has previously been applied to quantify collagen alignment in tendon (Miller et al. 2012; Wegner et al. 2017). Second harmonic generation (SHG) microscopy is used to directly visualize collagen fibre and sarcomeric structure in muscle tissue (Plotnikov et al. 2006a; Chen et al. 2012). This work identifies how the basic structure of the ECM relates to the mechanical function of muscle tissue. These parameters may be used to improve models of muscle passive stiffness that have proven challenging across muscles and disease states. The additional parameters of ECM architecture are utilized to improve understanding of the determinants of skeletal muscle stiffness, particularly in fibrotic diseases where excessive stiffness limits functionality.

Materials and methods

Ethical approval

All animal experiments were approved by the University of California, Davis Institutional Animal Care and Use Committee (protocol #20815). All experiments conformed to the guidelines set forth in the Guide for Care and Use of Laboratory Animals (National Research Council, 2011; Grundy 2015).

Animal handling and muscle isolation

Seven-week-old DBA/2J and D2.B10-Dmd*mdx*/J mice were obtained from The Jackson Laboratory. The mice were housed and bred in the UC Davis Teaching and Research Animal Care Services facility. They were grouped and housed on a 12:12 light–dark cycle, and

had *ab libitum* access to food and water. The mice (wildtype $N = 10$, dystrophic $N = 10$) were between 16 and 19 weeks of age when muscles were isolated. The mice were initially anaesthetized in a chamber with 2.5% isoflurane gas in 1 l/min of oxygen and then transferred to a nosecone that maintained 2.5% isoflurane at 1.5 l/min. After isolating the muscles in the lower limbs, the mice were killed by cervical dislocation while under anaesthesia. The extensor digitorum longus (EDL) and soleus (SOL) were stored in Ringer's solution with bubbling oxygen immediately after isolation and during mechanical protocols. After the muscles had undergone both passive and active mechanical studies, muscles from the right limb were flash-frozen in liquid nitrogen and stored at −80°C, and the muscles from the left side were pinned at approximate L_o and fixed in 4% paraformaldehyde for 24 h, then stored in phosphate-buffered saline (PBS) at 4°C. After killing, the diaphragm was removed, with one strip being flash-frozen and one strip fixed in 4% paraformaldehyde.

Active muscle mechanics

Passive and active mechanical protocols were performed using the EDL and soleus muscles. After isolation, the muscles were placed in a petri dish with Ringer's solution and bubbling O_2. 7-0 sutures were tied at the myotendinous junctions with loops that were then attached to the 300C-LR Dual-Mode motor arm and force transducer (Aurora Scientific) in a bath of Ringer's solution with O_2 at 22°C (Petrof et al. 1993; Barton et al. 2005). Optimum muscle length (L_o) was determined by performing twitches as the muscle was slowly stretched using the 701C high power follow stimulator (Aurora Scientific), with the length set at the largest twitch amplitude (Moorwood et al. 2013). The length (L_o) was taken using a caliper between the proximal and distal myotendinous junctions. The muscle length as well as muscle mass (m), ratio of fibre length to optimal muscle length (L_f/L_o), and density ($P = 1.06$ g/cm^3) were used to calculate the muscle physiological cross-sectional area (Mendez & Keys, 1960):

$$\mathrm{PCSA} = \mathrm{m} / [\mathrm{Lo} \times (\mathrm{Lf} / \mathrm{Lo}) \times \rho]$$

The active mechanical protocol consisted of measuring the maximum isometric twitch, followed 30 s later by a maximum isometric tetanus. This was repeated twice more with 5 min between each set. The maximum twitch and tetanus of the three trials was used in analysis. This protocol is based on a previous study (Smith & Barton, 2014).

Passive muscle mechanics

The strains performed during the passive mechanical protocol were determined from the L_o. Prior to each strain, the muscle was preconditioned by cyclical stretching to the given strain at 1 Hz for 5 s. After preconditioning, the muscle was strained 2.5% at 1 Lo/s and held for 2 min. Preconditioning, strain, and relaxation is repeated at 5, 7.5, 10 and 12.5% strain. The elastic stiffness is the tangent to the quadratic fit of elastic stress, which is the stress after 2 min of relaxation, at 10% strain. The elastic index is the ratio between elastic stiffness and dynamic stiffness, which is the tangent to the quadratic fit of the dynamic or maximum stress, at 10% strain (Smith & Barton, 2014). Any muscles that failed prior to 10% strain were excluded from any passive mechanical analysis. This technique is similar to other prior studies (Genet & 2014, n.d.; Burkholder & Lieber, 2001; Ward et al. 2009; Hakim et al. 2011; Smith & Barton, 2014).

Hydroxyproline assay

The hydroxyproline with collagen solubility assay was performed on the EDL, soleus, and diaphragm (DP) muscles similarly to prior studies (Flesch et al. 1997; Heydemann et al. 2005; Smith & Barton, 2014). Muscle mass was recorded prior to being rapidly frozen in liquid nitrogen and stored at −80°C until use. The tissue was powdered on dry ice using a mortar and pestle with careful attention to remove any remaining tendon. The powdered muscle was weighed, then was washed in 1 ml of PBS and stirred for 30 min at 4°C before centrifuging at 16,000 *g* for 30 min at 4°C. Non-crosslinked collagen was digested in a 1:10 (weight:volume) solution of 0.5 M acetic acid with 1 mg/ml pepsin, stirring overnight at 4°C. After centrifuging at 16,000 *g* for 30 min at 4°C, the supernatant was collected as the pepsin-soluble fraction (PSF), and the pellet was kept as the pepsin-insoluble fraction (PIF). The PSF and PIF were both hydrolysed overnight in 0.5 ml of 6 M hydrochloric acid at 105°C. Ten microlitres of hydrolysate were mixed with 150 μl isopropanol followed by 75 μl of 1.4% chloramine-T (ThermoFisher) in acetate citrate buffer and oxidized at room temperature for 10 min. The samples were then mixed with 1 ml of a 3:13 solution of Ehrlich's reagent (1.5 g of 4-(dimethylamino) benzaldehyde (ThermoFisher); 5 ml ethanol; 337 μl sulfuric acid) to isopropanol and incubated for 30 min at 58°C. Quantification was determined by extinction measurement of the resulting solution at 550 nm. A standard curve (0–1000 μM trans-4-hydroxy-L-proline; Fisher) was included in each assay. Results are reported as micrograms of hydroxyproline per milligram of tissue mass after powdering.

Histological collagen architecture

Picrosirius red staining was performed similarly to previous studies (Acuña et al. n.d.; Trensz et al. 2010; Ardite et al. 2012; Smith & Barton, 2014). Samples were blotted, weighed, fixed in 4% paraformaldehyde overnight, and then stored in PBS at 4°C until use. Prior to sectioning, muscles were placed in 4% agarose gel. Longitudinal sections of 200 μm thickness were cut using a Leica VT1000S. Sections were rinsed, air-dried for 1 h, and stained for 1 h in 0.1% (wt/vol) Direct Red 80 (Fisher) dissolved in saturated aqueous picric acid (Fisher). Sections were then washed in two 1 min rinses of 0.5% acetic acid, dehydrated in three 1 min changes of 100% ethanol, cleared with CitriSolv (Fisher Scientific) for 3 min, and mounted with Permount (Fisher Scientific).

A complete longitudinal section was captured by tiling images using a 20× objective with brightfield illumination on a Leica DMi8 microscope and DFC9000GTC camera. To evaluate collagen alignment, muscle sections were also viewed under linearly polarized light by inserting a rotating polarizer into the beam path before and after the section, respectively. A series of 10 tiling arrays were captured at angles from 0 to 90° in 10° increments.

A custom script was written in MATLAB (Mathworks) to evaluate the parameters of collagen architecture. Briefly, the birefringent light intensity reaches a maximum at 45° from the angle of collagen molecules (Fig. 1). The amplitude of intensity changes through the range of angles relates to the degree of structural alignment at a sub-pixel level. Thus, the mean of each pixel's amplitude was used to quantify the microECM alignment. The variability across pixels in the angle of maximum intensity was quantified using the circular

standard deviation and labelled macroECM deviation. Pixels that did not reach a threshold of average intensity were excluded from analysis.

Second harmonic generation microscopy collagen architecture

Muscles were blotted, weighed, fixed in 4% paraformaldehyde overnight, and then stored in PBS at 4°C. Prior to sectioning, muscles were placed in 4% agarose gel. Longitudinal sections were sliced at a thickness of 200 μm using a Leica VT1000s vibratome (Leica) and stained with WGA Oregon Green (Fisher) and RedDot 2 nuclear stain (Biotium). Images were taken on the Leica TCS SP8, equipped with a Mai Tai deep see laser for multiphoton microscopy, at the Advanced Imaging Facility in the UC Davis School of Veterinary Medicine. Images were taken with a 25× water immersion objective with the multiphoton laser tuned to 870 and 830 nm in sequence. Three image stacks per muscle were obtained with a depth of 100 μm and slice thickness of 1 μm.

A custom script in MATLAB was used to analyse the image stacks. First, the collagen SHG signal was separated from the sarcomeric SHG signal by combining multiple filtering methods (Fig. 2). First, the relative SHG intensity of 870:830 nm incident light was used to distinguish collagen and sarcomeres. Second, a Fourier transform was applied to calculate the sarcomere length, muscle fibre angle, and also filter based on the regularly spaced sarcomeres. Third, the angle of the fibres was used to filter based on an approximate fibre object. In limited cases with a less robust sarcomeric signal, fibre angle and sarcomere length were determined manually to facilitate filtering based on a fibre object without the Fourier transform filter. Any remaining sarcomeres in the collagen image were manually removed along with any imaging artefacts to create a muscle ECM image stack.

A maximum projection of the ECM image stack was created and contrast adjusted. OrientationJ was used to calculate the orientation of collagen within the image (Rezakhaniha et al. 2012; Püspöki et al. 2016). The mean deviation of the collagen fibres relative to the muscle fibres, or mean deviation, was quantified using the formula:

$$\delta = \sum_{j=1}^{n} (\alpha_j - f) \times p_j \tag{1}$$

The mean deviation δ is equal to the sum of the differences between each orientation angle α_j and the fibre angle f, multiplied by the corresponding proportion of pixels with that orientation p_j. We also calculated the mean collagen angle using the following formula:

$$\bar{\alpha} = \frac{1}{2} * atan2\left(\sum_{j=1}^{n} P_j \times \cos 2\alpha_j, \sum_{j=1}^{n} P_j \times \sin 2\alpha_j\right) \tag{2}$$

The mean collagen angle $\bar{\alpha}$ is equal to one half of the arctangent of the sum of the cosines and the sines of twice the orientation angles α_j multiplied by the number of pixels at that angle P_j. The mean deviation of the collagen from the mean collagen angle was calculated using eqn (1) with the replacement of the fibre angle with the mean collagen angle. There

was little difference between mean deviation from mean collagen angle and mean deviation from myofibre angle. Both were analysed, but the mean deviation from mean collagen angle, referred to as the collagen deviation, is reported. The difference between the mean collagen angle and the myofibre angle is reported as the myofibre–collagen angle.

The collagen fibre area percentage was also calculated within a custom MATLAB script. The ECM stack from the SHG separation code was processed through an intensity and coherence filter consistent with OrientationJ. The number of pixels that passed over all slices was divided by the total number of pixels with positive signal to remove any section of the stack that was not within tissue.

Statistical analysis

Image analysis was conducted blind to genotype of the mouse. Analysis was conducted using a two-way ANOVA within GraphPad Prism on muscle (EDL or soleus) and genotype (wildtype or *mdx*). *Post hoc* tests were performed to identify differences between individual groups using Sidak's multiple testing correction. Pearson's correlation coefficients and significance values were calculated between parameters. Significance was set at $P < 0.05$. Stepwise linear regression was performed using MATLAB on functional parameters with ECM parameters acting as modelling parameters. The significance to enter the model was set to $P < 0.10$ and the significance to exit at $P > 0.20$.

Results

Muscle size and mechanical properties

The functional impact of the adult dystrophic mice was determined by the maintenance of muscle and whole-body mass as well as the ability of muscles to generate active force while limiting passive stiffness. Male body mass was greater than female as expected across genotype; however, the *mdx* male had a significantly reduced body mass compared with wildtype males while there was no difference for female mice (Male: WT: 28.36 ± 2.19 g, *mdx*: 24.34 ± 1.63 g, $P = 0.031$; Female: WT: 21.24 ± 2.53 g, *mdx*: 20.44 ± 2.86 g, $P = 0.838$) (Fig. 3A). The loss in body mass is not attributable solely to the affected skeletal muscle as muscle weight to body weight ratio was not reduced for either EDL or soleus muscle (EDL: WT: 0.445 ± 0.089 mg/g, *mdx*: 0.437 ± 0.070 mg/g, $P = 0.8169$; SOL: WT: 0.383 ± 0.076 mg/g, *mdx*: 0.445 ± 0.070 mg/g, $P = 0.0790$)) (Fig. 3B). The muscle length was not reduced either, in either muscle, while muscle shortening is a reported feature of some human muscle contractures (EDL: WT: 10.982 ± 0.800 mm, *mdx*: 10.99 ± 0.715 mm, $P = 0.9833$; SOL: WT: 10.682 ± 0.823 mm, *mdx*: 10.617 ± 1.029 mm, $P = 0.8652$) (Fig. 3C). As expected, the ability of dystrophic muscle to generate normalized active tension was reduced, although the decrease in the soleus did not reach significance individually (EDL: WT: 10.795 ± 2.513 N/cm^2, *mdx*: 6.36 ± 2.298 N/cm^2, $P = 0.0007$; SOL: WT: 8.76 ± 3.844 N/cm^2, *mdx*: 6.565 ± 1.381 N/cm^2, $P = 0.0732$) (Fig. 3D). The defect in tetanic force-generating capacity of *mdx* muscles was not present in the half rise-time measure of twitch activation (EDL: WT: 13.45 ± 2.229 ms, *mdx*: 13.7 ± 2.700 ms, $P = 0.8173$; SOL: WT: 17.65 ± 2.274 ms, *mdx*: 17.6 ± 2.378 ms, $P = 0.9631$) (Fig. 3E). Interestingly, the relaxation kinetics were disrupted in the *mdx* soleus muscles; which became more moderate

in predominately slow muscle in relation to wildtype, with little change in EDL (EDL: WT: 33.60 ± 8.286 ms, *mdx*: 42.45 ± 8.438 ms, $P = 0.0809$; SOL: WT: 111.7 ± 16.83 ms, *mdx*: 77.3 ± 7.903 ms, $P < 0.0001$) (Fig. 3F). Inverse of specific tension, the *mdx* EDL muscle was significantly stiffer than wildtype muscle while the elastic stiffness of the soleus muscle was unchanged by dystrophy (EDL: WT: 156.65 ± 42.27 kPa, *mdx*: 330.85 ± 127.46 kPa, $P = 0.0001$; SOL: WT: 181.25 ± 87.10 kPa, *mdx*: 147.833 ± 55.00 kPa, $P = 0.6397$) (Fig. 3G). While both a purely elastic stiffness and a dynamic stiffness were measured, the ratio between them (elastic index) was unchanged (Fig. 3H) for dystrophic muscles in either EDL or soleus muscle (EDL: WT: 0.515 ± 0.047, *mdx*: 0.522 ± 0.060, $P = 0.9381$; SOL: WT: 0.483 ± 0.036, *mdx*: 0.471 ± 0.050, $P = 0.8404$).

Collagen content and crosslinking

In order to relate the mechanical properties to parameters of fibrosis, the extent of fibrotic collagen was quantified. The *mdx* muscles had more collagen than wildtype muscles, but the increase was only significant for the soleus and diaphragm muscles (EDL: WT: 9.793 ± 2.792 mg/g, *mdx*: 13.111 ± 3.579 mg/g, $P = 0.3646$; SOL: WT: 12.299 ± 4.103 mg/g, *mdx*: 18.732 ± 5.944 mg/g, $P = 0.0164$; DP: WT: 14.337 ± 3.491 mg/g, *mdx*: 37.150 ± 8.100 mg/g, $P < 0.0001$) (Fig. 4A). Crosslinking of collagen increases the mechanical stiffness of collagen and the resistance to degradation, thus increased collagen insolubility is an indicator of collagen crosslinking. The amount of crosslinked insoluble collagen increased in *mdx* compared with wildtype in all muscles. However, in the soleus the increase was proportional to the total collagen content, hence the insoluble collagen fraction and degree of crosslinking was consistent between genotypes. In contrast, the insoluble collagen fraction was significantly increased in *mdx* EDL compared with wildtype, representing increased collagen crosslinking (EDL: WT: 49.968 ± 8.168%, *mdx*: 68.137 ± 6.934%, $P = 0.0004$; SOL: WT: 61.937 ± 9.849%, *mdx*: 65.962 ± 16.38%, $P = 0.7397$; DP: WT: 76.167 ± 7.083%, *mdx*: 92.875 ± 1.126%, $P = 0.0080$) (Fig. 4B). Consistent with previous reports, increased total collagen content did not scale with increased elastic stiffness for either EDL or soleus muscles across wildtype and *mdx* mice (Fig. 4C). However, since *mdx* EDL muscles displayed increased stiffness while *mdx* soleus muscles demonstrated increased total collagen, there was a negative relationship between elastic stiffness and total collagen across *mdx* muscles (*mdx*: $R^2 = 0.3154$, $P = 0.012$), opposing the presumed relationship. On the other hand, an increase in stiffness of the *mdx* EDL can be attributed in significant proportion to the increase in collagen crosslinking of the *mdx* EDL (EDL: $R^2 = 0.2558$, $P = 0.023$), while in the soleus there was little relation of crosslinking to stiffness (Fig. 4D). The similarity in size between EDL and soleus enables more direct comparisons of mechanical and ECM architectural features, but the diaphragm is the most severely fibrotic muscle (Stedman et al. 1991). Indeed, the DBA/2J background shows a prominent collagen build-up in *mdx* diaphragm muscles that also includes a dramatic decrease in collagen solubility or increase in crosslinking (Fig. 4A,B). These results demonstrate that collagen crosslinking, distinct from total amount of collagen, is in part responsible for increased stiffness of fibrotic *mdx* muscles compared to wildtype.

Polarized light determination of ECM architecture

Beyond the biochemical makeup of collagen in skeletal muscle is the manner in which the linear collagen molecules align relative to the axis of the fibres. Picrosirius red-stained longitudinal muscle sections were imaged under rotating angles of linearly polarized light to capture the degree of collagen alignment (Fig. 1). MicroECM alignment is how ordered the sub-pixel ECM is (Fig. 5A), while macroECM deviation is a measure of the spread of alignment directions across pixels (Fig. 5B). Surprisingly, the degree of microECM alignment was not altered in fibrotic muscle (EDL: WT: 1.455 ± 0.173 AU, *mdx*: 1.353 ± 0.265 AU, $P = 0.4364$; SOL: WT: 1.399 ± 0.182 AU, *mdx*: 1.444 ± 0.137 AU, $P = 0.8468$) (Fig. 5C). Correspondingly, there was no relationship between the degree of elastic stiffness and microECM alignment across conditions (Fig. 5E). Similarly, macroECM deviation was consistent across muscles and genotype (EDL: WT: 10.114±2.095°, *mdx*: 12.075±3.281°, $P = 0.1521$; SOL: WT: 10.482±2.099°, *mdx*: 8.438±2.006°, $P = 0.1312$) (Fig. 5D). However, in wildtype muscles the expected association of decreasing axial elastic stiffness with increasing deviation in macroECM deviation was observed to be highly significant (WT: $R^2 = 0.3971$, $P = 0.003$) (Fig. 5F). Notably, in *mdx* muscle the relationship was abolished, with the slope inverted from the wildtype case indicating a fundamental alteration in the relationship between architecture and stiffness.

Second harmonic generation determination of collagen fibre architecture

In order to directly visualize the large collagen fibres of skeletal muscle and ECM in 3D, SHG microscopy was used to image thick tissue sections (Fig. 6A). Both collagen and sarcomeres produce an SHG signal, allowing determination of the sarcomere length at which collagen architecture was obtained. The sarcomere length was consistent across genotypes, but was elevated in soleus muscle (EDL: WT: 2.339 ± 0.275 μm, *mdx*: 2.348 ± 0.137 μm, $P = 0.9480$; SOL: WT: 2.529 ± 0.403 μm, *mdx*: 2.647 ± 0.345 μm, $P = 0.3951$) (Fig. 6E). A series of filtering steps were conducted in MATLAB to separate the sarcomeric signal from that of collagen and then collapsed into two dimensions for quantification of fibre orientation relative to the muscle fibre axis (Fig. 6B). Only relatively large collagen fibres are depicted by SHG, consistent with collagen perimysial cables visualized with electron microscopy rather than the endomysium that surrounds individual fibres (Gillies & Lieber, 2011). The EDL had significantly more area of SHG visual collagen fibres, but surprisingly the fibrotic *mdx* muscles did not show a significant increase in this highly organized collagen (EDL: WT: 0.316 ± 0.243%, *mdx*: 0.593 ± 0.709%, $P = 0.1220$; SOL: WT: 0.120 ± 0.167%, *mdx*: 0.166 ± 0.147%, $P = 0.7940$) (Fig. 6C). While fibrotic ECM may be presumed to be less organized than healthy ECM, the collagen fibres demonstrated less deviation (i.e. more alignment) in the *mdx* muscles than the wildtype (main effect of genotype $P = 0.005$, muscle $P = 0.274$, interaction $P = 0.5159$ by two-way ANOVA) (EDL: WT: 29.266 ± 5.689°, *mdx*: 24.617 ± 7.562°, $P = 0.2112$; SOL: WT: 32.831 ± 5.129°, *mdx*: 25.535 ± 6.847°, $P = 0.0296$) (Fig. 6D). Collagen fibre networks are known to orient along the direction of stretch (Girton et al. 2002; Vader et al. 2009), such that greater strain measured by sarcomere length would be expected to decrease the variation in collagen angles. Indeed, the SHG data show a significant relationship across muscle groups between sarcomere length and collagen deviation, which was more prevalent in the soleus (All: $R^2 = 0.1425$, $P = 0.016$; SOL: $R^2 = 0.2848$, $P = 0.015$) (Fig. 6G). Generally,

the collagen aligns with the myofibre as demonstrated by small collagen–myofibre angles, which is independent of muscle or genotype (EDL: WT: 6.789 ± 5.221°, *mdx*: 6.029 ± 2.804°, $P = 0.7715$; SOL: WT: 7.423 ± 2.394°, *mdx*: 9.200 ± 10.074°, $P = 0.5096$) (Fig. 6F). Across all muscle groups the collagen fibre area was significantly correlated to the elastic stiffness (All: $R^2 = 0.150$, $P = 0.015$) (Fig. 6H), implicating collagen fibres as important mechanical structures. This relationship was also significant without the data point at (2.46, 374), which seemed like an outlier initially (All: $R^2 = 0.1145$, $P = 0.038$). Strain stiffening models predict that the greater the degree of collagen alignment with the direction of stretch, the greater the stiffening along the axis of stretch becomes (Motte & Kaufman, 2013; Wang et al. 2015). Consistent with this we observed that as muscles were arbitrarily more stretched, as indicated by longer sarcomere lengths, the collagen deviation decreased (Fig. 6G). Critically, we show that collagen deviation is significantly related to muscle tissue dynamic and elastic stiffness (Fig. 6I), which is more tightly coupled in the EDL muscles that become excessively stiff in *mdx* mice (All: $R^2 = 0.1330$, $P = 0.023$, EDL: $R^2 = 0.2478$, $P = 0.026$). Our work demonstrates that SHG can be used to separate collagen and sarcomere signals allowing quantification of ECM architecture; which allowed demonstration of a hypothesized relationship between collagen fibres and their orientation with tissue stiffness.

Functional and ECM architectural parameter relationships

The novel parameters of ECM architecture measured in conjunction with mechanical properties allows the investigation of unique relationships between them. There is generally a degree of high correlation between parameters within group, muscle size, active and passive mechanics, and ECM architecture measured biochemically, by polarized light or SHG (Fig. 7). This can be a strong positive correlation such as between insoluble collagen content and collagen percentage insolubility that is expected based on the parameters. Notably, microECM alignment is inversely correlated with macroECM deviation, indicating an agreement across scales that increases confidence in novel measures. This was also the case in independent measures of collagen alignment with a significant correlation between macroECM deviation by polarized light and collagen fibre deviation by SHG. In some cases, the significant correlation is a product of the different muscles tested. For example, given that EDL has a lower fibre length to muscle length ratio (L_f/L_m), the physiological cross-sectional area (PCSA) is larger in EDL than soleus despite similar muscle mass and length. Given that EDL is a fast muscle this leads to the highly significant relationship between activation time and PCSA. Interestingly, specific force was inversely related to the amount of collagen and particularly insoluble collagen, consistent with the idea that collagen content can take up what would otherwise be contractile material. Sarcomere length is somewhat arbitrarily set as the muscle is pinned for imaging analysis, but showed correlation with many factors including PCSA, elastic index, twitch activation time, and macroECM deviation. The objective of the current study is to determine the factors that contribute to passive muscle stiffness, given its functional importance in people with muscle fibrosis. Notably, the only parameters with a significant correlation across all muscles was collagen fibre area and collagen fibre deviation, as previously described (Fig. 6H,I). Multiple linear regression analysis was performed to determine whether consideration of multiple ECM parameters simultaneously could improve the relationship to mechanical properties

or were overlapping. For elastic stiffness, collagen fibre area was the first parameter to enter and was followed by collagen deviation and macroECM deviation (Collagen deviation (°): −6.1084 ± 2.428, $P = 0.017$; Collagen fibre area (%): 85.841 ±38.545, $P = 0.032$; macroECM deviation (°): 14.631 ± 6.157, $P = 0.023$; Intercept (kPa): 199.79 ± 83.066, $P = 0.022$) (Fig. 7B). Combined, these three variables account for approximately one third of the variability in stiffness across muscle groups. The collagen deviation parameter was the most significant parameter within the model, marking it as a critical determinant of muscle stiffness. Surprisingly, while collagen deviation and collagen fibre area had negative and positive relationships with stiffness as hypothesized, macroECM deviation had a positive relationship with stiffness in the model. This highlights the difference in structures more broadly labelled with polarized light compared with the collagen fibres in SHG, even though they were significantly related to each other. For specific tension, however, the best predictor was insoluble collagen, consistent with just more assembled collagen taking up space that would otherwise be occupied by contractile myofibres (Insoluble collagen (μg/mg): −0.315 ± 0.112, $P = 0.008$; macroECM deviation (°): −0.483 ± 0.193, $P = 0.017$; Sarcomere length (μm): −2.894 ± 0.193, $P = 0.082$; Intercept (N/cm^2): 22.896 ± 5.273, $P = 0.0001$) (Fig. 7C). There was a less robust negative relationship with macroECM deviation, implying that more aligned ECM led to higher contractile force. A weak relationship was also present with sarcomere length but interpretation is tenuous, based on sarcomere length being set arbitrarily by pinning length. Multiple linear regression analysis was also performed within muscle type and within genotype for both elastic stiffness and specific tension. In all subgroups no more than one ECM parameter entered the model. This makes the model redundant with linear regression with the most highly related ECM parameter for the subset specific. These relationships between muscle function and ECM properties show for the first time how aspects of collagen architecture scale with muscle stiffness and contraction.

Discussion

In this study we have demonstrated a relationship between the architecture of the ECM and the increased passive muscle stiffness that occurs in fibrotic muscle diseases. Utilizing the *mdx* mutation on a DB2 background to produce stiff and fibrotic muscle, we developed novel image processing pathways to quantify ECM architecture. These techniques demonstrated a robust relationship between collagen fibres and their alignment with passive mechanical stiffness; previously unknown in skeletal muscle. While the degree of fibrosis is commonly quantified by collagen content, implying that increased collagen content reduces tissue functionality, we further demonstrate that this is not the case in skeletal muscle; and show that the manner in which collagen is organized is more impactful on muscle function. This link between architecture and function supports investigation of therapeutic strategies to target collagen architecture to facilitate passive muscle function in fibrotic muscle diseases.

Fibrosis is a common pathological consequence of many types of tissue damage and associated with nearly 45% of mortalities in the United States (Wynn, 2004). Fibrosis is associated with tissue stiffening in many tissues (Wells, 2013; Tschumperlin et al. 2018) and in skeletal muscle this stiffness is directly related to function. Skeletal muscle fibrosis is prominent across neuromuscular disorders and many are associated with contractures,

where excessive muscle stiffness limits or even abolishes joint mobility (Halar et al. 1978; Nuckolls et al. 2020). However, the common assumption that the increased fibrotic material, i.e. collagen, is directly related to the stiffness has been shown not to be the case as we further demonstrate here (Smith & Barton, 2014; Smith et al. 2019; Lieber & Fridén, 2019), though in tendon and collagen gels the alignment of collagen along the axis of stretch has been demonstrated as a key parameter of stiffness (Miller et al. 2012; Riggin et al. 2014; Wang et al. 2015; Taufalele et al. 2019). Here, we adapted polarized light microscopy with picrosirius red labelling of collagen used in tendon to analyse the alignment of collagen in skeletal muscle for the first time. Since collagen only makes up a small portion of skeletal muscle as opposed to tendon, we analysed 200 μm thick tissue sections to capture a greater degree of collagen structure than typical sections. We also probed the alignment at both the macro-, and micro-scale. The macro-scale collagen alignment was highly correlated to muscle stiffness; however, that relationship broke down in fibrotic *mdx* muscles. This indicates a rearrangement of the functional relationships between ECM architecture and stiffness in dystrophic muscle. Surprisingly, however, the macroECM deviation was not changed for either *mdx* muscle. The degree of collagen crosslinking could contribute to changes in stiffness distinct from the collagen content or alignment, particularly with crosslinking previously shown to be enhanced in dystrophic muscle (Smith et al. 2016). For the EDL muscle, collagen crosslinking was able to account for a significant amount of the increased stiffness in *mdx*. However, it had no relation to soleus muscle stiffness. This is consistent with collagen crosslinking being a poor predictor of muscle stiffness (Chapman et al. 2015). While being quantitative, these methods do not allow for a direct visualization of mechanically critical large collagen fibres and their architecture.

We utilized SHG imaging, which is ideally suited for muscle due to the native signal produced by sarcomeres and collagen (Plotnikov et al. 2006a; Chen et al. 2012). This also presents a challenge of separating those signals, which we overcame by combining multiple image processing techniques (Liu et al. 2013; Green et al. 2017; Salick et al. 2020). The collagen observed is not consistent with endomysial collagen as there is not a signal surrounding individual muscle fibres (Gillies & Lieber, 2011). Instead, large collagen fibres are visualized, consistent with the description of perimysial cables typically observed using electron microscopy (Gillies & Lieber, 2011; Gillies et al. 2017). While these perimysial cables have been suggested to be major contributors to passive stiffness (Gillies et al. 2017; Smith et al. 2019), the use of SHG microscopy allowed a more robust imaging of perimysial cables in conjunction with mechanical measurements. As hypothesized, the presence of more cables was related to increased stiffness, supporting their mechanical role. Critically, we also show that the alignment of these cables is significantly related to passive stiffness across genotypes and muscles, a general predictor of muscle stiffness. The techniques used could also provide empirical data to expand the capacity of current computational models of muscle stiffness (Marcucci et al. 2019; Bleiler et al. 2019). Collagen fibre alignment was indeed the most significant component of the ECM architecture-based model of muscle stiffness. SHG imaging in muscle has been primarily focused on the sarcomeres present (Plotnikov et al. 2006b; Dubreuil et al. 2018). It has also been used to investigate the structure of epimysial collagen in tissue-cleared muscles; however, the predominant circumferential direction perpendicular to that of functional stretch of muscle limits the

ability to interpret, along with negative longitudinal stiffness (Stearns-Reider et al. 2017). Here we have shown that SHG provides a powerful tool with which to further investigate the relationship between muscle fibres, collagen fibres and mechanics.

The relationship between ECM architecture and contractile function was explored in addition to passive function. The role of the ECM in muscle contraction is important for transmitting load (Ramaswamy et al. 2011). However, the manner in which it is perturbed in fibrosis is not consistent (Huebner et al. 2008; Gumucio et al. 2013). Our data show no relationship between imaging parameters and specific tension produced in muscles. Instead, specific tension was negatively correlated with total and insoluble collagen. This is consistent with a more straightforward presumption that fibrosis limits active contraction by taking up space from myofibrils. This is similar to previous studies in the *mdx* mouse (Smith & Barton, 2014), although in acute injury models specific tension has been shown to be more strongly related to fat rather than fibrotic infiltration of muscle (Biltz et al. 2020). The ECM architecture also had little bearing on contractile dynamics. The exceptions being that more variably aligned ECM was related to faster contraction while the presence of large collagen fibres was correlated with shortened relaxation times. A mechanical explanation of these relationships is difficult. Overall muscle contractile function in fibrotic muscle does appear to be related to the total amount of fibrotic material as opposed to its arrangement.

While fibrosis is prominent in muscle disease as well as in aging (Mann et al. 2011; Smith & Barton, 2018; Mahdy, 2019), the degree of fibrosis is not necessarily captured in animal models (Ng et al. 2012; Pessina et al. 2014). We used the *mdx* mutation on the DB2 background as it has been shown to produce a more fibrotic muscle (Fukada et al. 2010; van Putten et al. 2019). While there was an increase in collagen of the limb muscles analysed, the amount of fibrotic material was minor compared with the more severely impacted diaphragm (Stedman et al. 1991; Ragusa et al. 1996). However, the use of distinct, while similarly sized, limb muscles allows for direct comparisons across muscles for changes in ECM architecture and mechanical function of intact whole muscle. Duchenne muscular dystrophy is an X-linked disorder present predominantly in boys (Hoffman et al. 1987). Female *mdx* mice show a similar phenotype to males, albeit with a unique course of aging (Hourdé et al. 2013). In our studies, parameters normalized to size were not different between males and females, demonstrating a similar fibrotic response across sexes. Thus, other than body weight, analysis was performed across sexes. The *mdx* model provides a genetic tool for altering specific parameters of ECM architecture. However, as we have shown, many of these parameters are linked. Thus, a limitation of the current study is that it is correlative, and we are not able to test whether direct manipulation of collagen fibre alignment impacts passive tension. We do show a link between sarcomere length indicative of muscle strain and both macroECM deviation and collagen fibre alignment. While not possible with picrosirius red staining, an advantage of SHG microscopy is that it can be done without labels in live tissue (Webster et al. 2016; Lau et al. 2016). Feasibly, the collagen fibre alignment could be measured in live muscle across various strains to establish a more definitive relationship. Unfortunately, that is not possible with our current setup. The use of SHG does provide the ability to extend investigation of ECM architecture beyond animal models and into clinical populations. The alignment of collagen may be sensitive to shrinkage induced by the fixation protocol applied. As the muscles were fixed

at constant length, shrinkage would be expected to be cross-sectional (Cutts, 1988). Given that all muscles were fixed with the same protocol, any shifts in collagen alignment due to shrinkage would be anticipated to maintain difference in collagen alignment across samples. Extensive mechanical testing may also impact collagen alignment. Isometric contractions and a maximum strain of 12.5% for mechanical testing were used to limit potential muscle damage. Associated ECM architecture is thus expected to remain intact relative to the *in vivo* state.

We have demonstrated a relationship between ECM architecture and muscle passive mechanical properties. However, fibrotic muscle is also characterized by a lack of regeneration (Mann et al. 2011; Smith & Barton, 2018). The muscle stem cells responsible for regenerating new muscle tissue are known to be sensitive to the stiffness of their environment (Engler et al. 2004; Gilbert et al. 2010; Urciuolo et al. 2013). Muscle progenitors have also been shown to be sensitive to the alignment of their substrate (Zhao et al. 2009; Happe et al. 2017; Narayanan et al. 2020), making the study of *in vivo* alignment critical to understanding stem cell-based behaviours in muscle and how they are altered in fibrosis. A diverse assortment of cells assist muscle stem cells and may have unique sensitivities to architectural features of the ECM (Farup et al. 2015; Smith et al. 2018; Rubenstein et al. 2020). Here we demonstrate for the first time in skeletal muscle an array of parameters of ECM alignment using polarized light microscopy and SHG. The amount and alignment of collagen fibres or perimysial cables was found to be a general predictor of muscle passive stiffness, while the total amount of collagen had little relation to stiffness. This directs future research into anti-fibrotic therapies of skeletal muscle to investigate ECM architecture rather than the amount of fibrotic material in order to restore muscle function.

Supplementary Material

Refer to Web version on PubMed Central for supplementary material.

Acknowledgements

The SHG imaging was conducted at the UC Davis Health Sciences District Advanced Imaging Facility with support from Dr Ingrid Brust-Mascher. Assistance on separating the SHG signal from sarcomeres and collagen was provided by Dr Owen Carmichael and Dr David Burk from the Pennington Biomedical Research Center. We would like to thank Hyehyun Kim for contributions in imaging analysis that was vital to this work. We would like to also thank additional members of the MyoMatrix Lab at UC Davis, Linya Hu, CJ Mileti, Taryn Loomis and Matthew Nakaki, for thoughtful conversations and review of the data. Further acknowledgement of the lab of Dr Keith Baar for support in setting up experiments and attentive comments on the data.

Funding

This work was supported by a grant from the NIH National Institute of Arthritis and Musculoskeletal and Skin Diseases (NIAMS; R00AR067867).

Biography

Sarah E. Brashear graduated from UC Davis in 2018 with a B.S. in Neurobiology, Physiology, and Behavior and a minor in Mathematics. She joined Dr Smith's MyoMatrix Lab as a junior research specialist in late 2018. In October 2020, she became a graduate student at UC Davis in the Biomedical Engineering graduate group. After finishing her

master's degree, she would like to continue working in research, hopefully focusing on muscle diseases or orthopaedics.

Data availability statement

The data that support the findings of this study are openly available in figshare at https://doi.org/10.6084/m9.figshare.13099922.

References

Acuña MJ, Pessina P, Olguin H, Cabrera D, Vio CP, Bader M, Muñoz-Canoves P, Santos RA, Cabello-Verrugio C & Brandan E (2014). Restoration of muscle strength in dystrophic muscle by angiotensin-1-7 through inhibition of TGF-β signalling. Hum Mol Genet 23, 1237–1249. [PubMed: 24163134]

Ardite E, Perdiguero E, Vidal B, Gutarra S, Serrano AL & Muñoz-Cánoves P (2012). PAI-1-regulated miR-21 defines a novel age-associated fibrogenic pathway in muscular dystrophy. J Cell Biol 196, 163–175. [PubMed: 22213800]

Barton ER, Morris L, Kawana M, Bish LT & Toursel T (2005). Systemic administration ofL-arginine benefitsmdx skeletal muscle function. Muscle Nerve 32, 751–760. [PubMed: 16116642]

Bates G, Sigurdardottir S, Kachmar L, Zitouni NB, Benedetti A, Petrof BJ, Rassier D & Lauzon A-M (2013). Molecular, cellular, and muscle strip mechanics of the mdx mouse diaphragm. Am J Physiol - Cell Physiol 304, C873–C880. [PubMed: 23426972]

Biltz NK, Collins KH, Shen KC, Schwartz K, Harris CA & Meyer GA (2020). Infiltration of intramuscular adipose tissue impairs skeletal muscle contraction. J Physiol 598, 2669–2683. [PubMed: 32358797]

Bleiler C, Ponte Castañeda P & Röhrle O (2019). A microstructurally-based, multi-scale, continuum-mechanical model for the passive behaviour of skeletal muscle tissue. J Mech Behav Biomed Mater 97, 171–186. [PubMed: 31125890]

Bonnans C, Chou J & Werb Z (2014). Remodelling the extracellular matrix in development and disease. Nat Rev Mol Cell Biol 15, 786–801. [PubMed: 25415508]

Brynnel A, Hernandez Y, Kiss B, Lindqvist J, Adler M, Kolb J, van der Pijl R, Gohlke J, Strom J, Smith J, Ottenheijm C & Granzier HL (2018). Downsizing the molecular spring of the giant protein titin reveals that skeletal muscle titin determines passive stiffness and drives longitudinal hypertrophy. Elife 7:e40532. 10.7554/eLife.40532. [PubMed: 30565562]

Burkholder TJ & Lieber RL (2001). Review sarcomere length operating range of vertebrate muscles during movement.

Calvo B, Ramírez A, Alonso A, Grasa J, Soteras F, Osta R & Muñoz MJ (2010). Passive nonlinear elastic behaviour of skeletal muscle: Experimental results and model formulation. J Biomech 43, 318–325. [PubMed: 19857866]

Carríon JA, Torres F, Crespo G, Miquel R, García-Valdecasas J-C, Navasa M & Forns X (2010). Liver stiffness identifies two different patterns of fibrosis progression in patients with hepatitis C virus recurrence after liver transplantation. Hepatology 51, 23–34. [PubMed: 19839063]

Chapman MA, Pichika R & Lieber RL (2015). Collagen crosslinking does not dictate stiffness in a transgenic mouse model of skeletal muscle fibrosis. J Biomech 48, 375–378. [PubMed: 25529136]

Chen X, Nadiarynkh O, Plotnikov S & Campagnola PJ (2012). Second harmonic generation microscopy for quantitative analysis of collagen fibrillar structure. Nat Protoc 7, 654–669. [PubMed: 22402635]

Choi YA, Chun SM, Kim Y & Shin HI (2018). Lower extremity joint contracture according to ambulatory status in children with Duchenne muscular dystrophy. BMC Musculoskelet Disord 19, 287. 10.1186/s12891-018-2212-6. [PubMed: 30111310]

Cutts A (1988). Shrinkage of muscle fibres during the fixation of cadaveric tissue. J Anat 160, 75–78. [PubMed: 3253263]

Dubreuil M, Tissier F, Le Roy L, Pennec J-P, Rivet S, Giroux-Metges M-A & Le Grand Y (2018). Polarization-resolved second harmonic microscopy of skeletal muscle in sepsis. Biomed Opt Express 9, 6350–6358. [PubMed: 31065433]

Engler AJ, Griffin MA, Sen S, Bönnemann CG, Sweeney HL & Discher DE (2004). Myotubes differentiate optimally on substrates with tissue-like stiffness: pathological implications for soft or stiff microenvironments. J Cell Biol 166, 877–887. [PubMed: 15364962]

Farup J, Madaro L, Puri PL & Mikkelsen UR (2015). Interactions between muscle stem cells, mesenchymal-derived cells and immune cells in muscle homeostasis, regeneration and disease. Cell Death Dis 6, e1830–e1830. [PubMed: 26203859]

Flesch M, Schiffer F, Zolk O, Pinto Y, Rosenkranz S, Hirth-Dietrich C, Arnold G, Paul M & Böhm M (1997). Contractile systolic and diastolic dysfunction in renin-induced hypertensive cardiomyopathy. Hypertension 30, 383–391. [PubMed: 9314421]

Fratzl P, Misof K, Zizak I, Rapp G, Amenitsch H & Bernstorff S (1998). Fibrillar structure and mechanical properties of collagen. J Struct Biol 122, 119–122. [PubMed: 9724612]

Freundt JK & Linke WA (2019). Titin as a force-generating muscle protein under regulatory control. J Appl Physiol 126, 1474–1482. [PubMed: 30521425]

Fukada S-I, Morikawa D, Yamamoto Y, Yoshida T, Sumie N, Yamaguchi M, Ito T, Miyagoe-Suzuki Y, Takeda S, Tsujikawa K & Yamamoto H (2010). Genetic background affects properties of satellite cells and mdx phenotypes. Am J Pathol 176, 2414–2424. [PubMed: 20304955]

Genet MK-HM & 2014 undefined (n.d.). 1: Zou Y, Zwolanek D, Izu Y, Gandhy S, Schreiber G, Brockmann K, Devoto M, Tian Z, Hu Y, Veit G, Meier M, Stetefeld J, Hicks D, Straub V, Voermans NC.

Georges PC, Hui J-J, Gombos Z, McCormick ME, Wang AY, Uemura M, Mick R, Janmey PA, Furth EE & Wells RG (2007). Increased stiffness of the rat liver precedes matrix deposition: Implications for fibrosis. Am J Physiol - Gastro-intest Liver Physiol 293, G1147–G1154.

Gilbert PM, Havenstrite KL, Magnusson KEG, Sacco A, Leonardi NA, Kraft P, Nguyen NK, Thrun S, Lutolf MP & Blau HM (2010). Substrate elasticity regulates skeletal muscle stem cell self-renewal in culture. Science 329, 1078–1081. [PubMed: 20647425]

Gillies AR, Chapman MA, Bushong EA, Deerinck TJ, Ellisman MH & Lieber RL (2017). High resolution three-dimensional reconstruction of fibrotic skeletal muscle extracellular matrix. J Physiol 595, 1159–1171. [PubMed: 27859324]

Gillies AR & Lieber RL (2011). Structure and function of the skeletal muscle extracellular matrix. Muscle Nerve 44, 318–331. [PubMed: 21949456]

Girton TS, Barocas VH & Tranquillo RT (2002). Confined compression of a tissue-equivalent: Collagen fibril and cell alignment in response to anisotropic strain. J Biomech Eng 124, 568–575. [PubMed: 12405600]

Green NH, Delaine-Smith RM, Askew HJ, Byers R, Reilly GC & Matcher SJ (2017). A new mode of contrast in biological second harmonic generation microscopy. Sci Rep 7, 13331. 10.1038/s41598-017-13752-y. [PubMed: 29042656]

Grundy D (2015). Principles and standards for reporting animal experiments in The Journal of Physiology and Experimental Physiology. J Physiol 593, 2547–2549. [PubMed: 26095019]

Gumucio JP, Flood MD, Anthony CP, Brooks SV & Mendias CL (2013). Targeted inhibition of TGF-β results in an initial improvement but long-term deficit in force production after contraction-induced skeletal muscle injury. J Appl Physiol 115, 539–545. [PubMed: 23766498]

Hakim CH, Grange RW & Duan D (2011). The passive mechanical properties of the extensor digitorum longus muscle are compromised in 2-to 20-mo-old mdx mice. J Appl Physiol 110, 1656–1663. [PubMed: 21415170]

Halar EM, Stolov WC, Venkatesh B, Brozovich FFV & Harley JD (1978). Gastrocnemius muscle belly and tendon length in stroke patients and able-bodied persons. Arch Phys Med Rehabil 59, 476–484. [PubMed: 718411]

Happe CL, Tenerelli KP, Gromova AK, Kolb F & Engler AJ (2017). Mechanically patterned neuromuscular junctionsina-dish have improved functional maturation. Mol Biol Cell 28, 1950–1958. [PubMed: 28495800]

Herbert R (1988). The passive mechanical properties of muscle and their adaptations to altered patterns of use. Aust J Physiother 34, 141–149. [PubMed: 25026068]

Heydemann A, Huber JM, Demonbreun A, Hadhazy M & McNally EM (2005). Genetic background influences muscular dystrophy. Neuromuscul Disord 15, 601–609. [PubMed: 16084087]

Hoffman EP, Brown RH & Kunkel LM (1987). Dystrophin: the protein product of the duchenne muscular dystrophy locus. Cell 51, 919–928. [PubMed: 3319190]

Hourdé C, Joanne P, Noirez P, Agbulut O, Butler-Browne G & Ferry A (2013). Protective effect of female gender-related factors on muscle force-generating capacity and fragility in the dystrophic mdx mouse. Muscle Nerve 48, 68–75. [PubMed: 23625771]

Huebner KD, Jassal DS, Halevy O, Pines M & Anderson JE (2008). Functional resolution of fibrosis in mdx mouse dystrophic heart and skeletal muscle by halofuginone. Am J Physiol - Hear Circ Physiol 294, H1550–H1561.

Brown IE, Liinamma TL & Loeb GE (1996). Relationships between range of motion, lo, and passive force in five strap-like muscles of the feline hind limb. J Morphol 230, 69–77. [PubMed: 8843689]

Jones MG, Andriotis OG, Roberts JJ, Lunn K, Tear VJ, Cao L, Ask K, Smart DE, Bonfanti A, Johnson P, Alzetani A, Conforti F, Doherty R, Lai CY, Johnson B, Bourdakos KN, Fletcher SV, Marshall BG, Jogai S, Brereton CJ, Chee SJ, Ottensmeier CH, Sime P, Gauldie J, Kolb M, Mahajan S, Fabre A, Bhaskar A, Jarolimek W, Richeldi L, O'Reilly KM, Monk PD, Thurner PJ & Davies DE (2018). Nanoscale dysregulation of collagen structure-function disrupts mechano-homeostasis and mediates pulmonary fibrosis. Elife 7, e36354. [PubMed: 29966587]

Lake SP, Miller KS, Elliott DM & Soslowsky LJ (2009). Effect of fiber distribution and realignment on the nonlinear and inhomogeneous mechanical properties of human supraspinatus tendon under longitudinal tensile loading. J Orthop Res 27, 1596–1602. [PubMed: 19544524]

Lampi MC & Reinhart-King CA (2018). Targeting extracellular matrix stiffness to attenuate disease: from molecular mechanisms to clinical trials. Sci Transl Med 10, eaao0475. [PubMed: 29298864]

Lau J, Goh CC, Devi S, Keeble J, See P, Ginhoux F & Ng LG (2016). Intravital multiphoton imaging of mouse tibialis anterior muscle. IntraVital 5, e1156272. [PubMed: 28243520]

Lieber RL & Fridén J (2019). Muscle contracture and passive mechanics in cerebral palsy. J Appl Physiol 126, 1492–1501. [PubMed: 30571285]

Liu W, Raben N & Ralston E (2013). Quantitative evaluation of skeletal muscle defects in second harmonic generation images. J Biomed Opt 18, 26005. [PubMed: 23377006]

Magnusson SP, Simonsen EB, Aagaard P, Boesen J, Johannsen F & Kjaer M (2007). Determinants of musculoskeletal flexibility: viscoelastic properties, cross-sectional area, EMG and stretch tolerance. Scand J Med Sci Sports 7, 195–202.

Mahdy MAA (2019). Skeletal muscle fibrosis: an overview. Cell Tissue Res 375, 575–588. [PubMed: 30421315]

Mann CJ, Perdiguero E, Kharraz Y, Aguilar S, Pessina P, Serrano AL & Muñoz-Cánoves P (2011). Aberrant repair and fibrosis development in skeletal muscle. Skelet Muscle 1, 21. [PubMed: 21798099]

Marcucci L, Bondì M, Randazzo G, Reggiani C, Natali AN & Pavan PG (2019). Fibre and extracellular matrix contributions to passive forces in human skeletal muscles: An experimental based constitutive law for numerical modelling of the passive element in the classical Hill-type three element model. PLoS One 14, e0224232. [PubMed: 31689322]

Mathewson MA & Lieber RL (2015). Pathophysiology of muscle contractures in cerebral palsy. Phys Med Rehabil Clin N Am 26, 57–67. [PubMed: 25479779]

McDonald CM (1998). Limb contractures in progressive neuromuscular disease and the role of stretching, orthotics, and surgery. Phys Med Rehabil Clin N Am 9, 187–211. [PubMed: 9894140]

Mendez J & Keys A (1960). Density and composition of mammalian muscle. Metabolism 9, 184–188.

Meyer G & Lieber RL (2018). Muscle fibers bear a larger fraction of passive muscle tension in frogs compared with mice. J Exp Biol 221, jeb182089. [PubMed: 30237238]

Meyer GA, McCulloch AD & Lieber RL (2011). A nonlinear model of passive muscle viscosity. J Biomech Eng 133, 091007 10.1115/1.4004993. [PubMed: 22010742]

Miller KS, Connizzo BK, Feeney E & Soslowsky LJ (2012). Characterizing local collagen fiber re-alignment and crimp behavior throughout mechanical testing in a mature mouse supraspinatus tendon model. J Biomech 45, 2061–2065. [PubMed: 22776688]

Miyamoto N, Hirata K, Miyamoto-Mikami E, Yasuda O & Kanehisa H (2018). Associations of passive muscle stiffness, muscle stretch tolerance, and muscle slack angle with range of motion: individual and sex differences. Sci Rep 8, 8274 10.1038/s41598-018-26574-3. [PubMed: 29844513]

Moorwood C, Liu M, Tian Z & Barton ER (2013). Isometric and eccentric force generation assessment of skeletal muscles isolated from murine models of muscular dystrophies. J Vis Exp 10.3791/50036.

Motte S & Kaufman LJ (2013). Strain stiffening in collagen i networks. Biopolymers 99, 35–46. [PubMed: 23097228]

Myers BS, Woolley CT, Slotter TL, Garrett WE & Best TM (1998). The influence of strain rate on the passive and stimulated engineering stress-large strain behavior of the rabbit tibialis anterior muscle. J Biomech Eng 120, 126–132. [PubMed: 9675691]

Narayanan N, Jiang C, Wang C, Uzunalli G, Whittern N, Chen D, Jones OG, Kuang S & Deng M (2020). Harnessing fiber diameter-dependent effects of myoblasts toward biomimetic scaffold-based skeletal muscle regeneration. Front Bioeng Biotechnol 8, 10.3389/fbioe.2020.00203.

National Research Council (US) Committee for the Update of the Guide for the Care and Use of Laboratory Animals. (2011) Guide for the Care and Use of Laboratory Animals. 8th edition. Washington (DC): National Academies Press (US), https://www.ncbi.nlm.nih.gov/books/NBK54050/.

Ng R, Banks GB, Hall JK, Muir LA, Ramos JN, Wicki J, Odom GL, Konieczny P, Seto J, Chamberlain JR & Chamberlain JS (2012). Animal models of muscular dystrophy. In Progress in Molecular Biology and Translational Science, pp. 83–111. Elsevier, B.V.

Norton GR, Tsotetsi J, Trifunovic B, Hartford C, Candy GP & Woodiwiss AJ (1997). Myocardial stiffness is attributed to alterations in cross-linked collagen rather than total collagen or phenotypes in spontaneously hypertensive rats. Circulation 96, 1991–1998. [PubMed: 9323091]

Nuckolls GH, Kinnett K, Dayanidhi S, Domenighetti AA, Duong T, Hathout Y, Lawlor MW, Lee SSM, Magnusson SP, McDonald CM, McNally EM, Miller NF, Olwin BB, Raghavan P, Roberts TJ, Rutkove SB, Sarwark JF, Senesac CR, Vogel LF, Walter GA, Willcocks RJ, Rymer WZ & Lieber RL (2020). Conference report on contractures in musculoskeletal and neurological conditions. Muscle Nerve 61, 740–744. [PubMed: 32108365]

Pessina P, Cabrera D, Morales MG, Riquelme CA, Gutiérrez J, Serrano AL, Brandan E & Muñoz-Cánoves P (2014). Novel and optimized strategies for inducing fibrosis in vivo: focus on duchenne muscular dystrophy. Skelet Muscle 4, 7. [PubMed: 25157321]

Petrof BJ, Stedman HH, Shrager JB, Eby J, Sweeney HL & Kelly AM (1993). Adaptations in myosin heavy chain expression and contractile function in dystrophic mouse diaphragm. Am J Physiol 265, C834–C841. [PubMed: 8214039]

Pingel J, Bartels EM & Nielsen JB (2017). New perspectives on the development of muscle contractures following central motor lesions. J Physiol 595, 1027–1038. [PubMed: 27779750]

Plotnikov S, Juneja V, Isaacson AB, Mohler WA & Campagnola PJ (2006a). Optical clearing for improved contrast in second harmonic generation imaging of skeletal muscle. Biophys J 90, 328–339. [PubMed: 16214853]

Plotnikov SV, Millard AC, Campagnola PJ & Mohler WA (2006b). Characterization of the myosin-based source for second-harmonic generation from muscle sarcomeres. Biophys J 90, 693–703. [PubMed: 16258040]

Püspöki Z, Storath M, Sage D & Unser M (2016). Transforms and operators for directional bioimage analysis: a survey. Adv Anat Embryol Cell Biol 219, 69–93. [PubMed: 27207363]

van Putten M, Putker K, Overzier M, Adamzek WA, Pasteuning-Vuhman S, Plomp JJ & Aartsma-Rus A (2019). Natural disease history of the D2-mdx mouse model for Duchenne muscular dystrophy. FASEB J 33, 8110–8124. [PubMed: 30933664]

Ragusa RJ, St. Chow CK, Clair DK & Porter JD (1996). Extraocular, limb and diaphragm muscle group-specific antioxidant enzyme activity patterns in control and mdx mice. J Neurol Sci 139, 180–186. [PubMed: 8856650]

Ramaswamy KS, Palmer ML, Van Der Meulen JH, Renoux A, Kostrominova TY, Michele DE & Faulkner JA (2011). Lateral transmission of force is impaired in skeletal muscles of dystrophic mice and very old rats. J Physiol 589, 1195–1208. [PubMed: 21224224]

Rezakhaniha R, Agianniotis A, Schrauwen JTC, Griffa A, Sage D, Bouten CVC, Van De Vosse FN, Unser M & Stergiopulos N (2012). Experimental investigation of collagen waviness and orientation in the arterial adventitia using confocal laser scanning microscopy. Biomech Model Mechanobiol 11, 461–473. [PubMed: 21744269]

Riggin CN, Sarver JJ, Freedman BR, Thomas SJ & Soslowsky LJ (2014). Analysis of collagen organization in mouse achilles tendon using high-frequency ultrasound imaging. J Biomech Eng 136, 021029 10.1115/1.4026285. [PubMed: 24356929]

Rubenstein AB, Smith GR, Raue U, Begue G, Minchev K, Ruf-Zamojski F, Nair VD, Wang X, Zhou L, Zaslavsky E, Trappe TA, Trappe S & Sealfon SC (2020). Single-cell transcriptional profiles in human skeletal muscle. Sci Rep 10, 1–15. [PubMed: 31913322]

Salick MR, Napiwocki BN, Kruepke RA, Knight GT, Ashton RS & Crone WC (2020). The scanning gradient Fourier transform (SGFT) method for assessing sarcomere organization and alignment. J Appl Phys 127, 194701.

Skalsky AJ & McDonald CM (2012). Prevention and management of limb contractures in neuromuscular diseases. Phys Med Rehabil Clin N Am 23, 675–687. [PubMed: 22938881]

Smith LR & Barton ER (2014). Collagen content does not alter the passive mechanical properties of fibrotic skeletal muscle in mdx mice. Am J Physiol Cell Physiol 306, C889–C898. [PubMed: 24598364]

Smith LR & Barton ER (2018). Regulation of fibrosis in muscular dystrophy. Matrix Biol 68–69, 602–615.

Smith LR, Cho S & Discher DE (2018). Stem cell differentiation is regulated by extracellular matrix mechanics. Physiology 33, 16–25. [PubMed: 29212889]

Smith LR, Hammers DW, Sweeney HL & Barton ER (2016). Increased collagen cross-linking is a signature of dystrophin-deficient muscle. Muscle Nerve 54, 71–78. [PubMed: 26616495]

Smith LR, Lee KS, Ward SR, Chambers HG & Lieber RL (2011). Hamstring contractures in children with spastic cerebral palsy result from a stiffer extracellular matrix and increased in vivo sarcomere length. J Physiol 589, 2625–2639. [PubMed: 21486759]

Smith LR, Pichika R, Meza RC, Gillies AR, Baliki MN, Chambers HG & Lieber RL (2019). Contribution of extracellular matrix components to the stiffness of skeletal muscle contractures in patients with cerebral palsy. Connect Tissue Res 1–12. 10.1080/03008207.2019.1694011. [PubMed: 30667273]

Stearns-Reider KM, D'Amore A, Beezhold K, Rothrauff B, Cavalli L, Wagner WR, Vorp DA, Tsamis A, Shinde S, Zhang C, Barchowsky A, Rando TA, Tuan RS & Ambrosio F (2017). Aging of the skeletal muscle extracellular matrix drives a stem cell fibrogenic conversion. Aging Cell 16, 518–528. [PubMed: 28371268]

Stedman HH, Sweeney HL, Shrager JB, Maguire HC, Panettieri RA, Petrof B, Narusawa M, Leferovich JM, Sladky JT & Kelly AM (1991). The mdx mouse diaphragm reproduces the degenerative changes of Duchenne muscular dystrophy. Nature 352, 536–539. [PubMed: 1865908]

Swift J, Ivanovska IL, Buxboim A, Harada T, Dingal PCDP, Pinter J, Pajerowski JD, Spinler KR, Shin J-W, Tewari M, Rehfeldt F, Speicher DW & Discher DE (2013). Nuclear lamin-A scales with tissue stiffness and enhances matrix-directed differentiation. Science 341, 1240104. [PubMed: 23990565]

Taufalele PV, VanderBurgh JA, Muñoz A, Zanotelli MR & Reinhart-King CA (2019). Fiber alignment drives changes in architectural and mechanical features in collagen matrices. PLoS One 14, e0216537. [PubMed: 31091287]

Trensz F, Haroun S, Cloutier A, Richter MV & Grenier G (2010). A muscle resident cell population promotes fibrosis in hindlimb skeletal muscles of mdx mice through the Wnt canonical pathway. Am J Physiol Physiol 299, C939–C947.

Tschumperlin DJ, Ligresti G, Hilscher MB & Shah VH (2018). Mechanosensing and fibrosis. J Clin Invest 128, 74–84. [PubMed: 29293092]

Urciuolo A, Quarta M, Morbidoni V, Gattazzo F, Molon S, Grumati P, Montemurro F, Tedesco FS, Blaauw B, Cossu G, Vozzi G, Rando TA & Bonaldo P (2013). Collagen VI regulates satellite cell self-renewal and muscle regeneration. Nat Commun 4, 1964. [PubMed: 23743995]

Vader D, Kabla A, Weitz D & Mahadevan L (2009). Strain-induced alignment in collagen gels. PLoS One 4, e5902. [PubMed: 19529768]

Wang H, Abhilash AS, Chen CS, Wells RG & Shenoy VB (2015). Long-range force transmission in fibrous matrices enabled by tension-driven alignment of fibers. Biophys J 107, 2592–2603.

Ward SR, Tomiya A, Regev GJ, Thacker BE, Benzl RC, Kim CW & Lieber RL (2009). Passive mechanical properties of the lumbar multifidus muscle support its role as a stabilizer. J Biomech 42, 1384–1389. [PubMed: 19457491]

Ward SR, Winters TM, O'Connor SM & Lieber RL (2020). Non-linear scaling of passive mechanical properties in fibers, bundles, fascicles and whole rabbit muscles. Front Physiol 11, 10.3389/fphys.2020.00211.

Webster MT, Manor U, Lippincott-Schwartz J & Fan C-M (2016). Intravital imaging reveals ghost fibers as architectural units guiding myogenic progenitors during regeneration. Cell Stem Cell 18, 243–252. [PubMed: 26686466]

Wegner KA, Keikhosravi A, Eliceiri KW & Vezina CM (2017). Fluorescence of picrosirius red multiplexed with immunohistochemistry for the quantitative assessment of collagen in tissue sections. J Histochem Cytochem 65, 479–490. [PubMed: 28692327]

Wells RG (2013). Tissue mechanics and fibrosis. Biochim Biophys Acta - Mol Basis Dis 1832, 884–890.

Wynn TA (2004). Fibrotic disease and the TH1/TH2 paradigm. Nat Rev Immunol 4, 583–594. [PubMed: 15286725]

Zhao Y, Zeng H, Nam J & Agarwal S (2009). Fabrication of skeletal muscle constructs by topographic activation of cell alignment. Biotechnol Bioeng 102, 624–631. [PubMed: 18958861]

Key points

- The amount of fibrotic material in dystrophic mouse muscles relates to contractile function, but not passive function.
- Collagen fibres in skeletal muscle are associated with increased passive muscle stiffness in fibrotic muscles.
- The alignment of collagen is independently associated with passive stiffness in dystrophic skeletal muscles.
- These outcomes demonstrate that collagen architecture rather than collagen content should be a target of anti-fibrotic therapies to treat muscle stiffness.

Translational perspective

Skeletal muscle fibrosis is prevalent across many muscle diseases, particularly in muscular dystrophy. Fibrosis is the build-up of extracellular matrix components, primarily collagen, which impairs tissue function. However, the mechanisms by which fibrosis limits muscle function are not well understood. By using a fibrotic dystrophic mouse model in conjunction with advanced imaging modalities to assess fibrotic tissue architecture we were able to provide evidence for structure–function relationships of the extracellular matrix in muscle. Our data support the replacement of contractile tissue with collagen as the primary mechanism for reduced muscle strength in fibrosis. Importantly, in contrast, the amount of fibrotic tissue was not a good predictor of passive muscle stiffness. In many fibrotic conditions passive muscle stiffness can limit range of motion around a joint leading to debilitating joint contractures. Our data provide evidence that instead of total collagen, the degree to which collagen is incorporated into large fibres and how well those fibres are aligned are the primary drivers of muscle stiffness. This motivates the development of therapies to target manipulation of collagen architecture for use in patients with contractures. This work also establishes pipelines for the imaging and analysis of collagen architecture in skeletal muscle tissue to further understand the role of fibrotic structure in limiting muscle function.

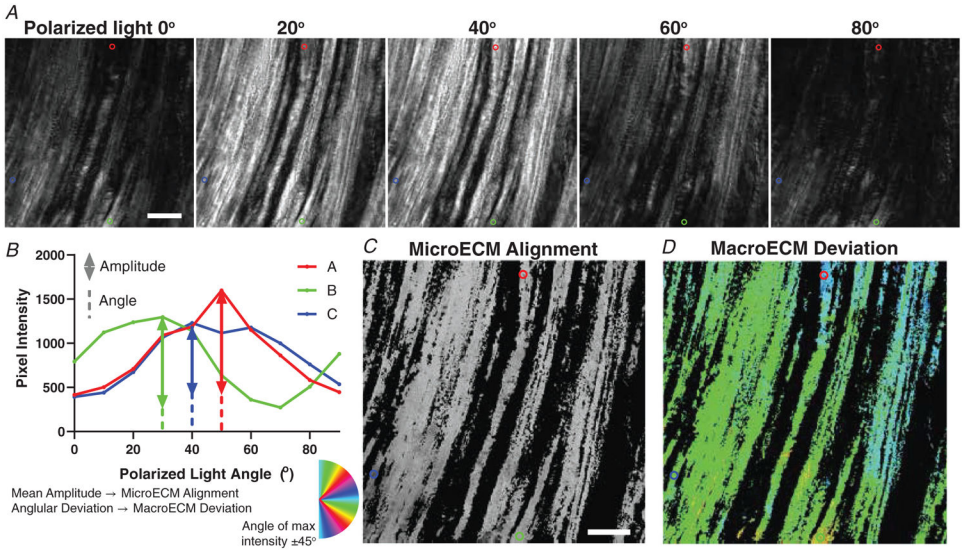

Figure 1. Polarized light picrosirius red imaging and analysis of ECM architecture

A, each muscle was imaged with a polarizer at the given angle and an analyser 90° from the polarizer. Images were taken at every 10° between 0° and 90°. The red, blue, and green circles are highlighting the same three pixels across all angles and analyses. *B*, example pixel intensities across the range of angles are demonstrated. The amplitude is used to determine the mean pixel microECM alignment. The circular standard deviation of the angle of maximum intensity is used to determine macroECM deviation. *C*, the image is scaled based on the mean amplitude (microECM alignment) of each pixel. *D*, the same image is represented by the angle of maximum intensity, with the primary orientation of the ECM being 45° from that angle as represented by the colour. The circular standard deviation across the muscle is used to calculate the macroECM. Pixels below an average intensity threshold were not included in *C* and *D* or the analysis. Scale bar = 100 μm.

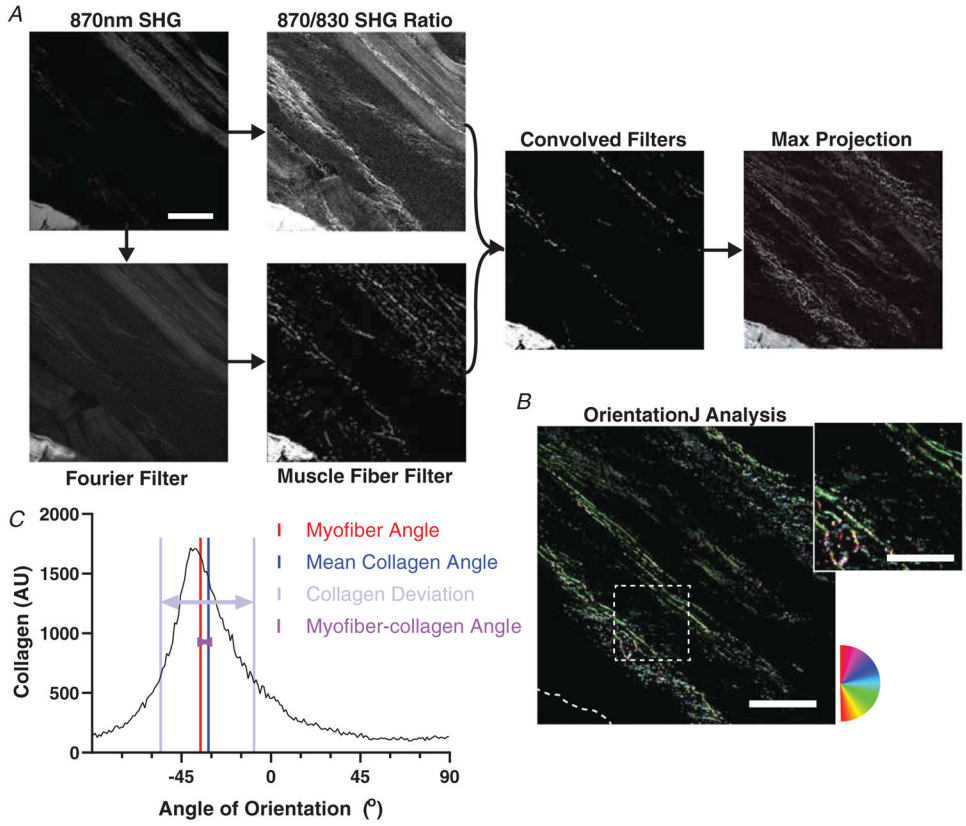

Figure 2. Second harmonic generation (SHG) image processing and analysis

A, flowchart of the SHG image processing code run in MATLAB. Representative images of each stage of processing shown. SHG Original Image was the raw image taken from the SHG microscope. SHG 870/830 Ratio was the result of rescaling the original image based on relative pixel intensities at 870 nm and 830 nm wavelengths. Fourier Transform is the result of using a Fourier transform to identify and remove sarcomeres from the SHG original image. Fibre filter is the result of removing fibre structures from the Fourier transform image. Convolved filters is the result of rescaling a combination of the fibre filter and SHG 870/830 Ratio images. Max projection is the result of taking the maximum intensity at each pixel location from the entire stack of convolved filter images, and compressing the stack into a single image (*A*). *B*, as for all images, any tendon or aponeurosis was removed manually as in the lower left portion. OrientationJ analysis and distribution was run to measure the frequencies of orientations present in the max projection. The inset shows a portion of the image with collagen fibres visible along with changing colour as orientation shifts according to the circular colour scale. *C*, the colour survey map is shown representing the histogram with orientation frequencies. The myofibre angle is depicted along with the circular average of the collagen angles. The myofibre–collagen angle is the difference between these two. The collagen deviation is a measure of the spread of the histogram from the mean collagen angle. Scale bar = 100 μm; inset = 50 μm.

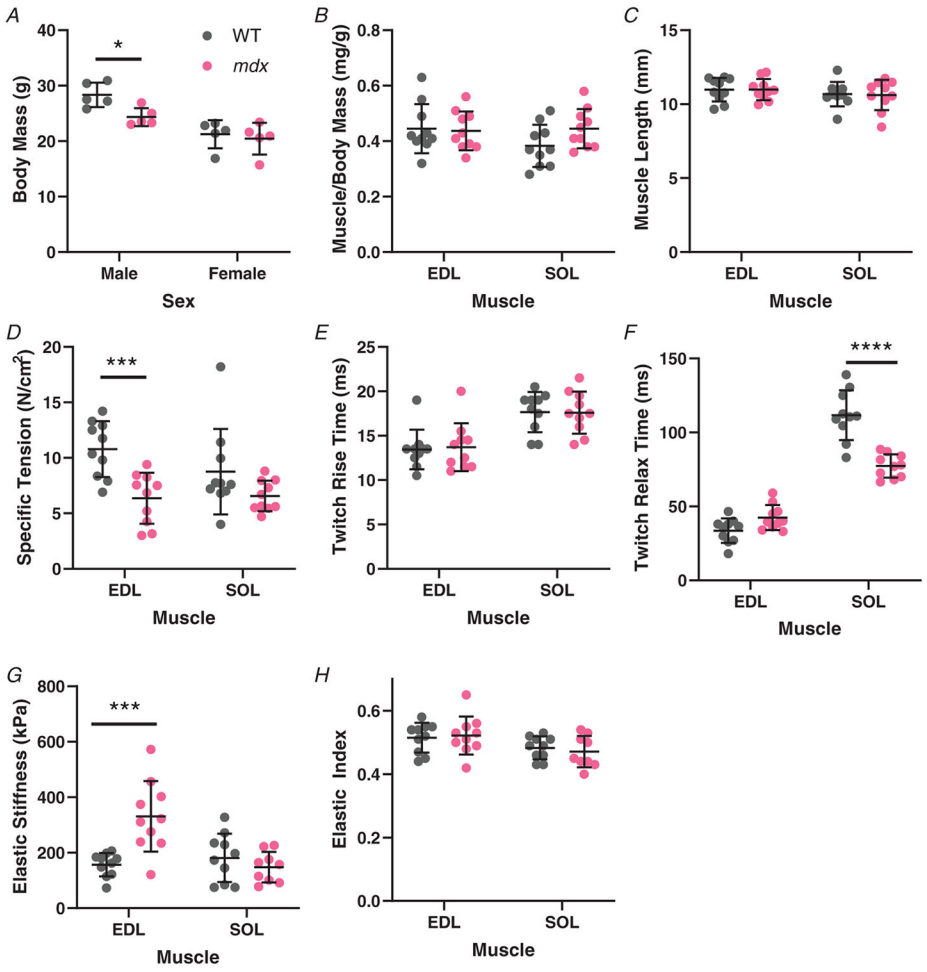

Figure 3. Muscle size and mechanical properties from wildtype (*n* = 10; 5M/5F) and *mdx* (*n* = 10; 5M/5F) mice

A, total body mass was greater for male mice than female mice. Body mass of *mdx* males is significantly lower than wildtype males. *B*, the ratio of individual muscle masses to body mass is consistent across genotypes along with similar mass between EDL and soleus. *C*, muscle length (L_o) was set at the length of peak twitch force. Muscle length was consistent across all groups. *D*, the specific force of *mdx* EDL was significantly lower than wildtype, with a similar trend in soleus muscle that did not reach significance. *E*, twitch rise-time to half of active peak twitch tension is more rapid in the EDL muscle than soleus corresponding to the predominantly fast and slow phenotypes, respectively. The genotype had no impact on activation kinetics. *F*, there are genotype and muscle-specific impacts on relaxation time for twitch force to reach half of peak tension. The *mdx* EDL had little difference from wildtype EDL, while the *mdx* soleus relaxes more quickly than the wildtype soleus. *G*, elastic stiffness taken as the elastic modulus at 10% strain shows the *mdx* EDL is significantly stiffer than the wildtype EDL. The soleus had similar stiffness between genotypes. *H*, the elastic index, related to the amount of force remaining after stress relaxation compared with the peak force, showed no effect in *mdx* muscle. As a whole, the EDL muscles were significantly more elastic than soleus. **P* < 0.05, ****P* < 0.001, and *****P* < 0.0001.

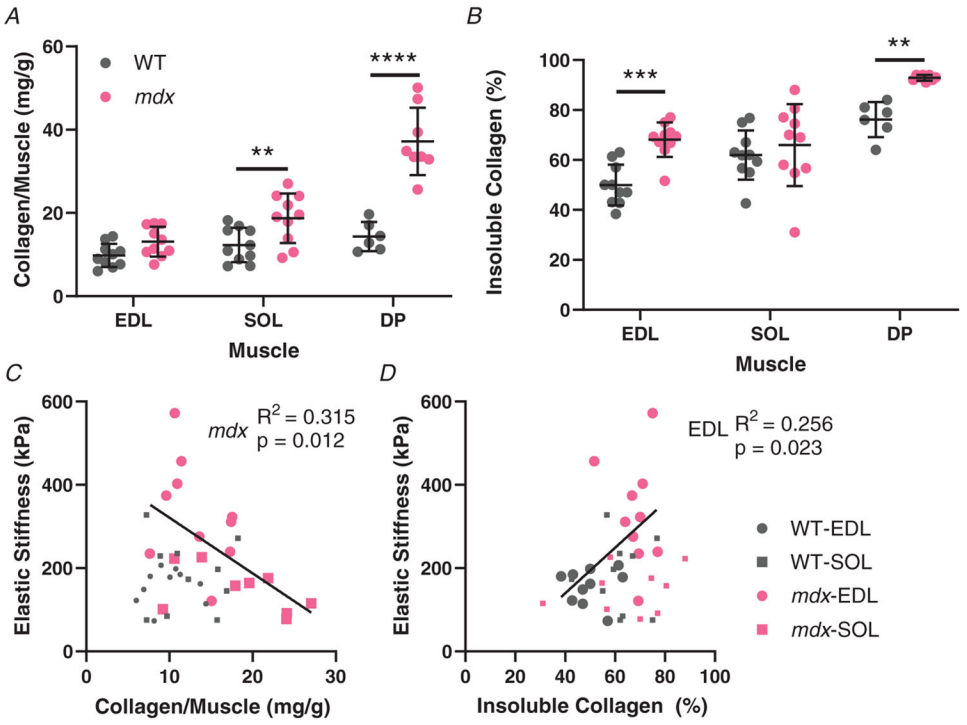

Figure 4. Collagen content and solubility, determined through a hydroxyproline assay, and its relation to passive mechanics

A, the amount of collagen per muscle in wildtype and *mdx* muscles. The soleus and especially diaphragm muscle collagen content of *mdx* mice was significantly increased compared with the wildtype. Diaphragm muscles were not collected from all mice (n = 6 wildtype; n = 8 *mdx*). *B*, the percentage of collagen that was pepsin insoluble as an indication of crosslinked collagen per muscle in wildtype and *mdx* muscles. Contrasting with total collagen, EDL muscle had significantly more crosslinked collagen compared while there was no difference in soleus. The diaphragm muscle was the most crosslinked with a highly significant increase in crosslinking in *mdx* diaphragms. *C*, the relationship between the amount of collagen per muscle and muscle elastic stiffness. There is a significant negative relationship for the *mdx* muscles, demonstrating that increased fibrotic material does produce stiffness in fibrosis. *D*, the relationship between elastic stiffness and collagen insolubility per muscle. The percentage of soluble collagen and elastic stiffness had a significant positive correlation, indicating a link between stiffness and crosslinking in the EDL. ** $P < 0.01$, *** $P < 0.001$ and **** $P < 0.0001$.

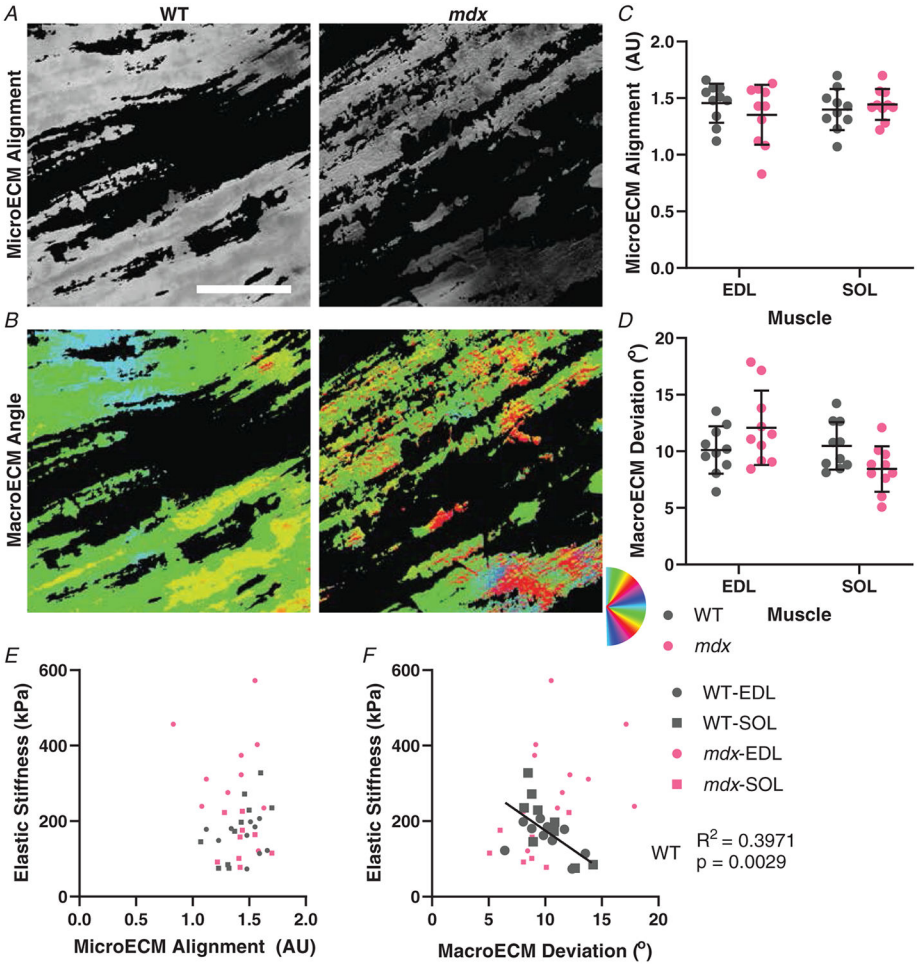

Figure 5. ECM orientation observed using picrosirius red stain and polarized light microscopy

A, example images from wildtype and *mdx* EDL muscles that show the microECM alignment. *B*, the same images depicting macroECM deviation with colours representing the angle of ECM orientation. *C*, the quantification of the microECM alignment shows no significant difference between genotypes in either muscle. *D*, the macroECM deviation shows no significant difference between genotypes in either muscle, with all groups having approximately 10° deviation. *E*, the microECM alignment was not significantly correlated with elastic stiffness overall or for any subgroup. *F*, the relationship between macroECM deviation and elastic stiffness showed a significant negative correlation in wildtype muscles that was not present in *mdx* muscles. Scale bar = 100 μm.

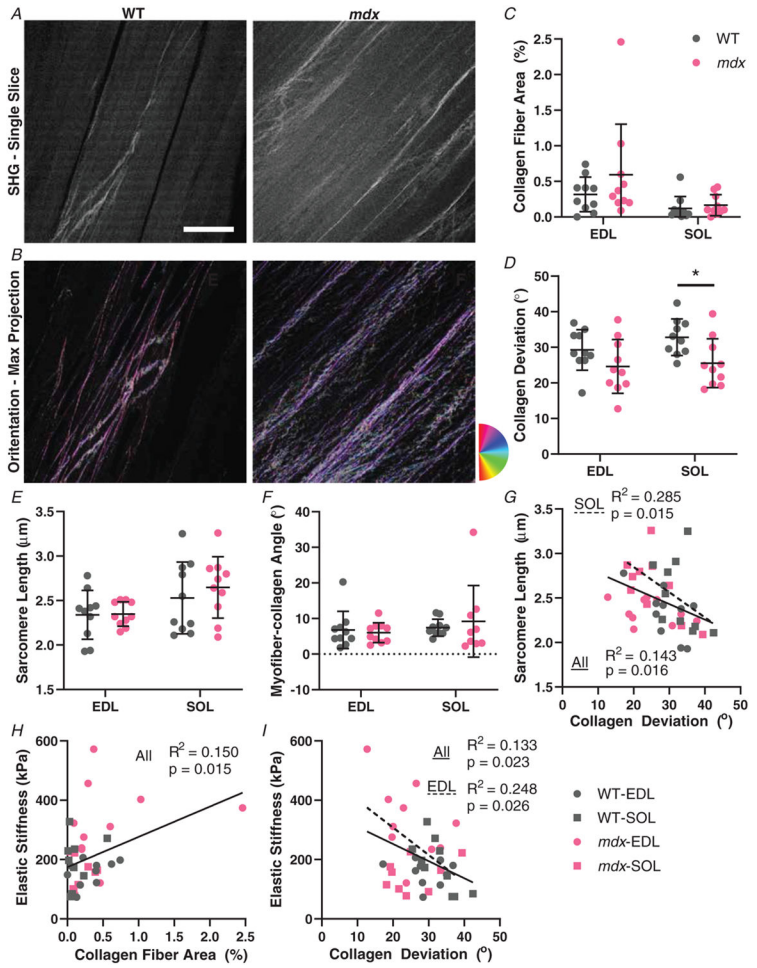

Figure 6. Collagen architecture determined using second harmonic generation (SHG) microscopy

A, example SHG images of a single slice of wildtype and *mdx* EDL muscles at 870 nm. *B*, a max projection of the stack with a colour map of the collagen fibre angles from OrientationJ from the same wildtype and *mdx* images as in (*A*). *C*, the number of collagen fibres visible with SHG was not significantly different in either muscle for *mdx*. The EDL had significantly more collagen fibres than soleus. *D*, collagen deviation was similar between EDL and soleus muscles. The *mdx* muscles had significantly lower deviation angle than the wildtype mice, with *post hoc* tests significant in soleus. *E*, sarcomere length determined from Fourier transform of SHG images. There is no significant difference in sarcomere length between wildtype and *mdx* mice for either muscle, but soleus had significantly longer sarcomere lengths than EDL. *F*, the angle between mean collagen angle and the myofibre angle was generally small (<10°) and did not significantly vary across muscle groups. *G*, all groups combined had a significant negative correlation of sarcomere length and collagen deviation angle. The soleus muscle had an independent significant negative correlation. *H*, there was a significant positive correlation between collagen fibre area and stiffness across all groups. *I*, there is also a relationship between collagen deviation and elastic stiffness. All groups combined had a significant negative correlation and the EDL muscle also had a significant negative correlation independently. $*P < 0.05$. Scale bar = 100 μm.

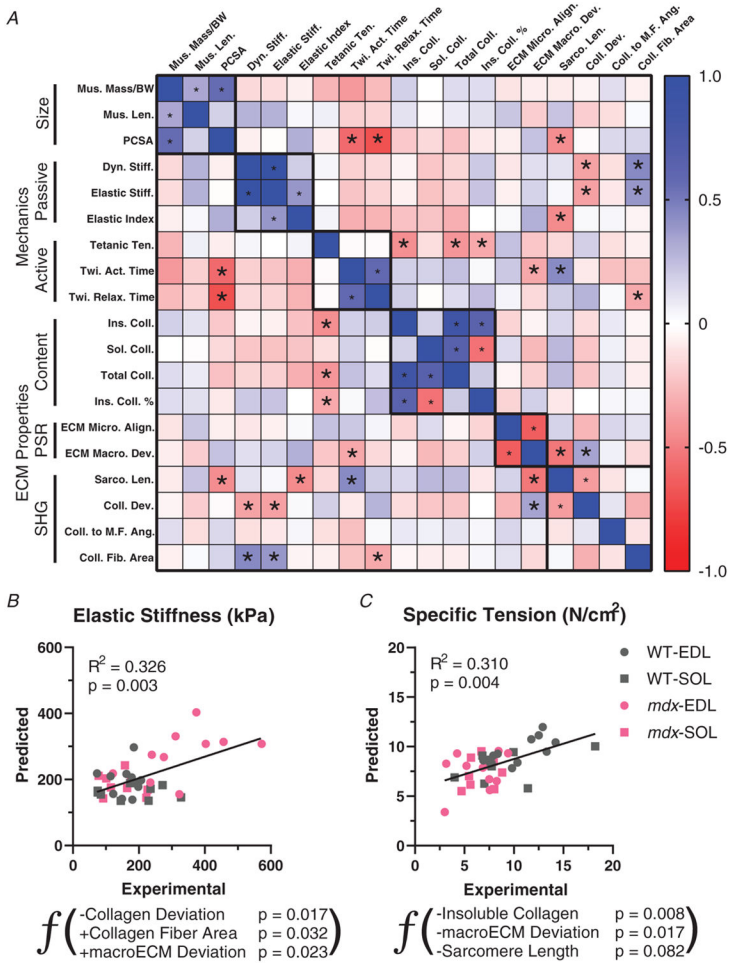

Figure 7. Relationships between muscle functional and ECM architectural parameters

A, correlation matrix based on parameters of muscle size, active and passive mechanics, and ECM architecture determined by collagen content, polarized light and second harmonic generation (SHG). Blue indicates positive Pearson's correlation coefficient values and red negative. $*P < 0.05$ indicates significant correlations. *B*, multiple linear regression analysis for elastic stiffness using ECM architectural properties as predictors. A negative relationship with collagen deviation was the most significant factor in the model. This is contrasted by a positive relationship with macroECM deviation. Higher collagen fibre area predicted greater elastic stiffness in the model. *C*, multiple linear regression analysis for specific tension using the same ECM architectural properties. Insoluble, i.e. crosslinked, collagen content was the most significant predictor of specific tension. The macroECM deviation had a negative relationship in the model, and sarcomere length was a modest negative predictor of specific tension.